JACS JOURNAL OF THE AMERICAN CHEMICAL SOCIETY

Article

Cite This: J. Am. Chem. Soc. 2017, 139, 15377-15384

pubs.acs.org/JACS

Self-Assembling Ability Determines the Activity of Enzyme-Instructed Self-Assembly for Inhibiting Cancer Cells

Zhaoqianqi Feng, Huaimin Wang, Xiaoyi Chen, and Bing Xu*

Department of Chemistry, Brandeis University, 415 South Street, Waltham, Massachusetts 02453, United States

Supporting Information

ABSTRACT: Enzyme-instructed self-assembly (EISA) represents a dynamic continuum of supramolecular nanostructures that selectively inhibits cancer cells via simultaneously targeting multiple hallmark capabilities of cancer, but how to design the small molecules for EISA from the vast molecular space remains an unanswered question. Here we show that the self-assembling ability of small molecules controls the anticancer activity of EISA. Examining the EISA precursor analogues consisting of an N-capped D-tetrapeptide, a phosphotyrosine residue, and a diester or a diamide group, we find that, regardless of the stereochemistry and the regiochemistry of their tetrapeptidic backbones, the anticancer activities of these precursors largely match their self-assembling abilities. Additional mechanistic studies confirm that the assemblies of the small peptide derivatives result in cell death, accompanying significant rearrangement of cytoskeletal proteins and plasma membranes. These results imply that the diester or diamide derivatives of the D-tetrapeptides self-assemble pericellularly, as well as intracellularly, to result in cell death. As the first case to correlate thermodynamic properties (e.g., self-assembling ability) of small molecules with the efficacy of a molecule process against cancer cells, this work provides an important insight for developing a molecular dynamic continuum for potential cancer therapy, as well as understanding the cytotoxicity of pathogenic assemblies.

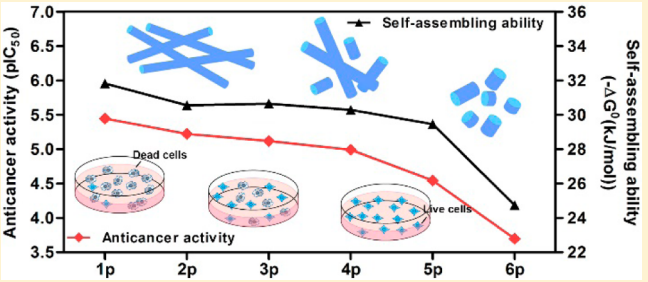

INTRODUCTION

Only approximately 3000 of the predicted ~30 000 genes in the human genome are coded for proteins that possess the ability of binding small druglike molecules.[1,2] Among the 3000 druggable genes, only 600−1500 are disease-associating genes that are potential drug targets.[1] The limited number of small-molecule drug targets urge the development of innovative approaches other than tight ligand−receptor binding.[3] As a complementary process for ligand−receptor interactions, enzyme-instructed self-assembly (EISA) is a ubiquitous phenomenon in cellular processes that affords spatiotemporal control of higher order structures from nanoscales to microscales.[4] Inspired by such a fundamental fact in cell biology, we and others are employing EISA of small molecules to develop new therapeutics,[5−7] especially for cancer therapy.[8−11] Generating supramolecular assemblies via EISA enables selective targeting of the undruggable targets or simultaneous interaction with multiple targets.[12] For example, alkaline phosphatase (ALP), being reported as a biomarker of cancer for about 5 decades,[13] remains undruggable due to the difficulties in achieving inhibitor selectivity and sufficient cell permeability.[14] Recently, we have selectively targeted such a undruggable feature on cancer cells via EISA of small peptides.[15] Moreover, the supramolecular assemblies formed via EISA not only inhibit cells via multiple mechanisms but also promise to prevent acquired drug resistance.[16] In addition, EISA provides an effective approach for targeting loss-of-function (i.e., silencing tumor suppressors) in cancer cells,[17] which ultimately may meet such a major challenge in translational medicine. Several other laboratories also pioneered the exploration of EISA for biomedical applications, including inhibiting cancer cells. For example, Pires et al. demonstrated using EISA of a carbohydrate derivative to selectively inhibit osteosarcoma cells that overexpress ALP.[18] Maruyame and co-workers employed a protease (e.g., MMP-7) to trigger molecular self-assembly of a peptide lipid and to induce cancer cell death through intracellular EISA.[19] Moreover, Liang and co-workers, combining EISA with GSH-controlled condensation, used one precursor to differentiate the extra- and intracellular environments to yield two different nanofibers via self-assembly.[20] Yang and colleagues demonstrated the use of enzyme-catalyzed hydrogel as an efficient adjuvant to boost immune response to a vaccine.[21] In addition, EISA also finds applications for photoacoustic imaging of furin-like activity[22] and monitoring autophagy.[23] Moreover, the concept of EISA is applicable to nanoparticles.[24] These studies not only expand the scope of precursors and enzymes utilized for EISA but also underscore the promises of EISA for a variety of biomedical applications.

Despite the promise of EISA in selectively inhibiting cancer cells or molecular imaging,[25] there are several important questions that remain to be answered. Of special significance is

Received: July 9, 2017
Published: October 9, 2017

DOI: 10.1021/jacs.7b07147
J. Am. Chem. Soc. 2017, 139, 15377−15384

how to design a small molecule for EISA. That is, what molecular feature (or thermodynamic property) is the most important factor for increasing the efficacy of EISA for various applications? Particularly in the case of small peptides, although it is conceivable to obtain the different activities of peptide assemblies by varying the residues, sequences, or capping group of peptides or peptide derivatives,[26] the relationship between the self-assembling ability of small molecules and the corresponding activity remains to be established, which is crucial for guiding the design of small molecule assemblies for anticancer therapy, as well as for other applications. To address this critical question, we designed and synthesized a series of structural analogues of peptidic precursors (Scheme 1) that differ in several key

Scheme 1. Molecular Structures of the Precursors and the Correlation between the Ability for Self-Assembly of Small Molecules and Anticancer Activity

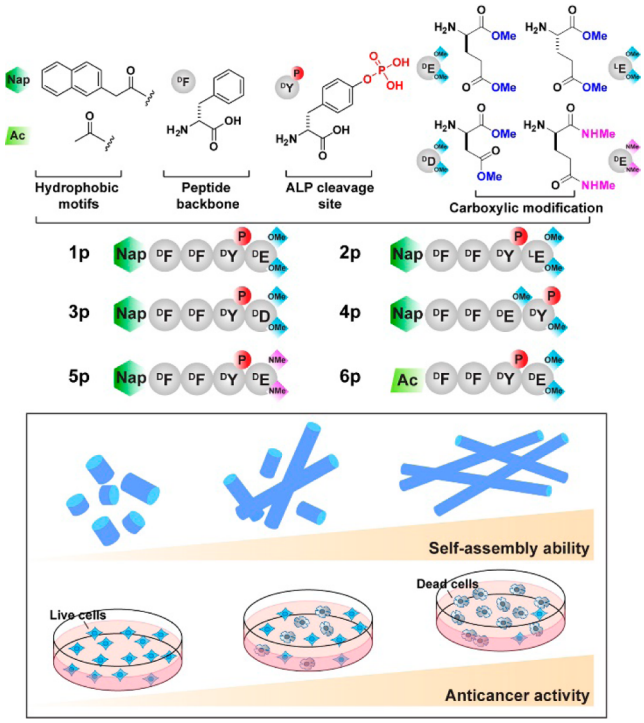

molecular features: C-terminal capping, stereochemistry, and regiochemistry. Our results indicate that the self-assembling abilities of these peptide derivatives dictate the anticancer activity of EISA for inhibiting cancer cells. That is, the precursors with higher self-assembling ability turn into the molecules (e.g., hydrogelators) that exhibit higher self-assembling ability, resulting in effective formation of assemblies that inhibit cancer cells. Cell imaging reveals that the assemblies of the small peptide derivatives likely affect the interactions between plasma membrane and cytoskeletons to result in cell death. Besides positively corroborating the inhibitory activity and self-assembling ability of small molecules, this work also provides insights for understanding in situ molecular self-assembly in cell milieu[27] and helps develop EISA as a molecular process for potential cancer therapy, as well as other biomedical applications.

RESULTS AND DISCUSSION

Molecule Design and Synthesis. On the basis of an anticancer precursor (**1p**)[28] of EISA and via fragment combination and the mutation of peptide sequences, we design a series of EISA precursors that consist of a peptidic backbone, an ALP cleavage site, a carboxylic modification, and an N-terminal capping (Scheme 1). The peptidic backbone D-Phe-D-Phe is the enantiomer of the well-studied dipeptide Phe-Phe, which forms nanocrystals[29] mainly stabilized by aromatic−aromatic interactions. The phosphotyrosine residue provides enzymatic cleavage site for ALP to generate supramolecular assemblies.[30] Because O-methylation of protein increases the hydrophobicity and neutralizes the negative charge of amino acid residues, which results in enhanced self-assembling ability[11] and nonspecific binding to cell membrane,[31] we choose to O-methylate the carboxylic acid groups in D-Glu, L-Glu, and D-Asp. The difference in stereochemistry of C-terminal amino acid residue (i.e., D-Glu and L-Glu) or in side-chain length (i.e., D-Glu and D-Asp) would verify whether conventional ligand−receptor binding contributes to the activities of the assemblies. Considering that the carboxyl ester is a substrate of esterase and a receptor of nucleophilic attack, we use *N*-methylacetamine (−CONHMe) as the C-terminal capping of the peptide. Thus, the difference between −COOMe and −CONHMe groups would delineate the contribution of the reactivity of the assemblies for the activities. Inspired by protein N-acetylation, a phenomenon that occurs in almost all eukaryotic proteins,[32] we cap the N-terminal of the precursors by a 2-naphthylacetyl group, since naphthyl groups provide strong intermolecular aromatic−aromatic interactions.

By systemically combining the aforementioned peptide backbone, N-terminal capping, and C-terminal modifications, we would generate five new precursors (Scheme 1, **2p**, **3p**, **4p**, **5p**, and **6p**). These precursors differ from **1p**[28] in terms of N-terminal capping, C-terminal modification, stereochemistry, or regiochemistry, which would help answer the following questions: (1) How do the structural differences (i.e., N-terminal capping, C-terminal modification, stereochemistry, and regiochemistry) affect the nanostructures of assemblies via EISA? (2) How do the self-assembling abilities of either the phosphorylated precursors or the dephosphorylated products determine the efficacy of EISA for inhibiting cancer cells?

The designed precursors and their corresponding self-assembling molecules are accessible via a facile synthetic route [Scheme S1, Supporting Information (SI)]. We first prepared phospho-D-tyrosine in 90% yield,[33] followed by the *N*-Fmoc protection, which yielded Fmoc-Tyr(PO_3H_2)-OH.[34] Following a general procedure for solid-phase peptide synthesis,[35] we synthesized N-terminal capped peptides with Fmoc-protected amino acids. Esterification of the carboxylic acid groups, catalyzed by trimethylsilyl bromide,[36] produced the O-methylated precursors. We directly coupled the carboxylic acids with methylamine to obtain the *N*-methylamide derivative (**5p**). NMR spectra and LC−MS confirmed the structures of precursors after high-performance liquid chromatography (HPLC) purified them.

Self-Assembling Ability in Vitro. To evaluate the self-assembly of the precursors and the corresponding self-assembling molecules in vitro, we employed transmission electron microscopy (TEM) to visualize the nanostructures formed by the precursors, at 0.5 wt %, before and after EISA occurs. As shown in Figure 1, dissolving in aqueous solution and bearing D-glutamic acid diester at its C-terminal, **1p** mainly forms short nanofibers with a width of 6 ± 2 nm and a length of 60 ± 10 nm, together with several thicker nanofibers with a diameter of 12 ± 2 nm. Containing L-glutamic acid diester and as a

DOI: 10.1021/jacs.7b07147
J. Am. Chem. Soc. 2017, 139, 15377−15384

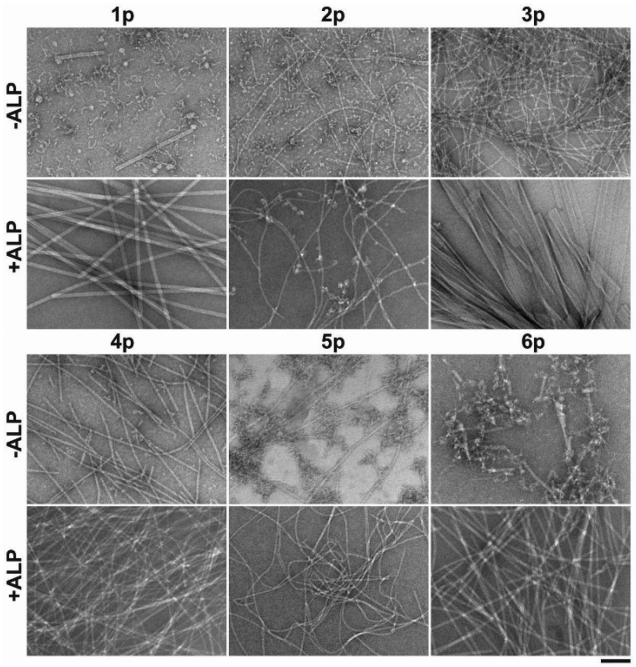

Figure 1. TEM images of the nanostructures formed by 0.5 wt % **1p**–**6p** in pH 7.4 water, before and after adding ALP (2 U/mL) (scale bar, 100 nm).

diastereomer of **1p**, **2p** results in nanofibers with a diameter the same as that of **1p** (i.e., 6 ± 2 nm), but the lengths of the nanofibers range from nanometers to micrometers. The replacement of D-glutamic acid diester with D-aspartic acid diester yields **3p**, which shows different self-assembly morphology, containing mainly longer fibers. These fibers are typically micrometers long and have a diameter of 6 ± 2 nm. The difference between **1p** and **3p** likely arises from the length of the side chain of the amino acid. Precursor **4p**, inserting the D-glutamic acid ester between the phenylalanine and tyrosine residues and having an O-methylated C-terminal, results in more uniform long fibers several micrometers in length and with widths of about 7 ± 2 nm. Using methyl amine as the C-terminal modification group produces **5p**, which forms nanofibers (6 ± 2 nm) interacting with amorphous aggregates. Using an acetyl group to replace a naphthyl motif in **1p** results in **6p**, which forms some big aggregates, together with thinner fibers (5 ± 2 nm in diameter) than those of **1p**–**5p**. The naphthyl-capped precursor (e.g., **1p**) has higher self-assembling ability than the acetyl-capped precursor (e.g., **6p**), verifying that naphthyl groups provide strong aromatic–aromatic interactions. These results indicate that the precursors self-assemble to form certain nanostructure when being dissolved in aqueous solution at a physiological pH and at relatively high concentration (0.5 wt %).

Upon the treatment with ALP, **1p** turns into **1**, which self-assembles to yield rigid nanofibers with a diameter of 14 ± 2 nm, similar as the previous observation.[28] After forming by dephosphorylation, **2**, **3**, or **4** self-assembles to form nanofibers with a diameter of 6 ± 2 nm, nanoribbons, and nanofibers with a diameter of 7 ± 2 nm, respectively, implying that stereochemistry, the side chain length, and regiochemistry all affect the morphologies of the self-assembled nanostructures generated by EISA. Unlike the case of **1p**, the EISA of **5p** generates long flexible nanofibers with diameters of 6 ± 2 nm, indicating that *N*-methylacetamide is less hydrophobic than the methyl ester at the C-terminal of the peptide and provides a slightly weaker self-assembling ability. Dephosphorylation of **6p** generates **6**, which forms straight nanofibers with a diameter of 9 ± 2 nm. Table 1 summarize the morphologies of the assemblies without or with the addition of ALP.

To more precisely evaluate the self-assembling ability in the context of EISA, we measured the critical micelle concentration (cmc) of the above precursors (**2p**–**6p**) and their corresponding self-assembling molecules (**2**–**6**) by using rhodamine 6G as a probe.[37] [Figures 2 and S16 and S17 (SI)] Compared with other

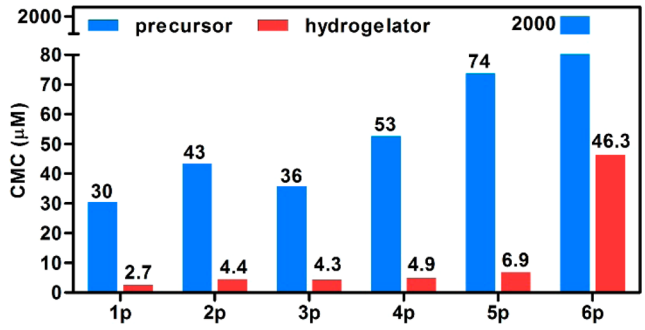

Figure 2. Cmc values of precursors **1p**–**6p** and their corresponding dephosphorylated peptide derivatives **1**–**6**.

precursors, **1p** bears the highest self-assembling ability (i.e., the lowest cmc of 30 μM[28]). The cmc values of **2p**–**4p** are higher than that of **1p**, indicating that the changes in the stereochemistry, side chain length, and regiochemistry all affect the self-assembling ability of the precursors. The cmc of **5p** is more than double of that of **1p**, indicating that the O-methylation of the tetrapeptide results in higher self-assembling ability than the N-methylamidation does. **6p** exhibits nearly 70-fold weaker self-assembling ability, which is consistent with the TEM results above. The cmc values of the precursors follow the order of **1p** < **3p** < **2p** < **4p** < **5p** < **6p**. The self-assembling abilities of the dephosphorylated molecules follow the trend of **1** > **3** > **2** > **4** > **5** > **6**, the same as that of the precursors. This result likely originates from the identical difference (i.e., phosphorylation) between the precursors and the self-assembling molecules. The TEM images reveal that there are hardly any nanostructures formed by the precursors at the concentration lower than the cmc of the corresponding self-assembling molecules, without or with the addition of ALP (Figure S18, SI). The correlation between the cmc and the fiber formation likely resembles the formation of worm micelles from micelles.[38] In fact, the size and

Table 1. Summary of the Self-Assembly of the EISA Molecules

compound[a]	**1p**	**2p**	**3p**	**4p**	**5p**	**6p**
morphology before adding ALP (d^b, nm)	fibers (6 ± 2, 12 ± 2)	fibers (6 ± 2)	fibers (6 ± 2)	fibers (7 ± 2)	aggregate, fibers (6 ± 2)	aggregate, fibers (5 ± 2)
morphology after adding ALP (d^b, nm)	fibers (14 ± 2)	fibers (6 ± 2)	nanoribbons	fibers (7 ± 2)	fibers (6 ± 2)	fibers (9 ± 2)

[a]The concentration is 0.5 wt %. [b]Diameter of nanofibers.

DOI: 10.1021/jacs.7b07147
J. Am. Chem. Soc. 2017, 139, 15377–15384

morphology of the assemblies of **1** depend on the concentration of **1** (Figure S19, SI), which supports this inference.

Anticancer Activity and Static Light Scattering. The assemblies formed via EISA are cytotoxic to cancer cells, while the monomers are innocuous,[7] suggesting the importance of the in situ self-assembling process for inhibiting cancer cells. These results prompt us to examine the correlation between the self-assembling ability of EISA molecules (i.e., the precursors and the self-assembling molecules) and their efficacy for inhibiting cancer cells. We choose an osteosarcoma cell line (Saos-2) as the cancer cells for the test because the high expression level of ALP on Saos-2 warrants fast dephosphorylation of the precursors.[18,39] The thermodynamic parameter ($-\Delta G^0$) characterizes the free energy change for formation of assemblies,[40] and the pIC_{50} values, which is $-\log_{10}(IC_{50})$,[41] represent the cytotoxicity of the precursors. As shown in Figure 3, the potency (pIC_{50}) of EISA

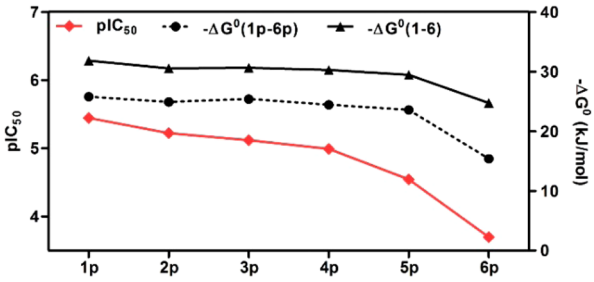

Figure 3. Correlation between the self-assembling ability ($-\Delta G^0$) and anticancer activity (pIC_{50}) of EISA molecules against Saos-2 cells.

precursors at 24 h against Saos-2 cells follows the order of **1p** > **2p** > **3p** > **4p** > **5p** > **6p**, exhibiting positive correlation with the self-assembling ability ($-\Delta G^0$) of the precursors (and the dephosphorylation products) except the relative order of **2p** and **3p**, which, nevertheless, are quite close in both potency and self-assembling ability. At the concentration of their IC_{50} values, the precursors (**1p**−**6p**) hardly form any nanostructures in aqueous solution. However, the addition of ALP into the above solutions results in irregular fibrous structures, indicating the formation of assemblies via EISA at these concentrations (Figure S21, SI). While all the designed molecules assemble into fibrous structures, these nanostructures differ slightly in morphology. We speculate that the differences between the morphologies of the nanostructures may marginally contribute to the subtle cytotoxicity differences between the EISA molecules. In fact, the IC_{50} values of the precursors correlate with the cmc values of corresponding self-assembling molecules, indicating that the in situ formation of assemblies plays a critical role in inhibiting cancer cells. These results suggest that the self-assembling ability of EISA precursors and their self-assembling products determine the potency of EISA against cancer cells.

The positive correlation between the self-assembling ability of the molecules for EISA and their anticancer efficacy suggests that the amounts of assemblies generated in situ (i.e., on or inside cancer cells) may be critical in inhibiting the cancer cells. To test this hypothesis, we measured the static light scattering (SLS) of the solutions of three representative precursors (i.e., **1p**,[28] **5p**, and **7p**[28]) (Scheme S2, SI) before and after the addition of ALP, since the signal intensity is proportional to the amount of assembly. We choose to compare these precursors because they share the same backbone structure and only differ in the modification of the carboxylic group, which is methyl ester for **1p**, methyl amide for **5p**, and carboxylic acid for **7p**. As shown in Figure 4A, the light-scattering results show that the increase of the SLS signal depends on the concentrations of the precursors.

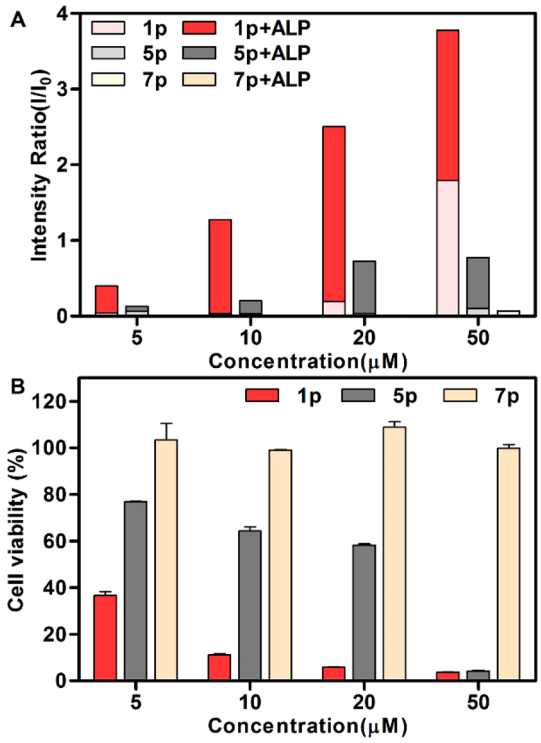

Figure 4. (A) Intensity of static light scattering (SLS) of the solutions of **1p**, **5p**, and **7p** (5−50 μM) before and after adding ALP (1 U/mL) for 12 h in pH 7.4 PBS buffer (light-scattering angle = 60°). (B) The cell viability of Saos-2 cells treated with **1p**, **5p**, or **7p** (5−50 μM) for 24 h.

The SLS signal of **1p** increases from 0.04 to 1.80 as the concentration rises from 5 to 50 μM, indicating that more assemblies formed at higher concentrations. The solutions of **5p** and **7p** exhibit little SLS signal, even at the concentration of 50 μM, suggesting that the precursors hardly form any assemblies at these concentrations, which is consistent with their cmc results [Figures 2 and S16 and 17 (SI)]. The addition of ALP to the solution of **1p** and **5p** causes significant increase of the SLS signals, confirming the generation of assemblies via EISA. However, the ALP treatment shows little effect on the solution of **7p**, likely due to the weak self-assembling abilities of **7p** and **7**. After ALP treatment, the signal intensity of the solutions of the precursors follows the order of **1p** > **5p** > **7p**, confirming that the amounts of assemblies of **1**, **5**, and **7**, formed via EISA at the initial concentration of 5 μM or 50 μM, follow the trend of **1** > **5** > **7**.

To correlate the concentration of the assemblies with inhibition efficacy, we also tested the cell viabilities of Saos-2 cells treated with **1p**, **5p**, or **7p** within these two concentrations, 5 and 50 μM (Figure 4B). The cell viability results show that **1p** and **5p** exhibit cytotoxicity in a dose-dependent manner, while **7p** is innocuous to Saos-2 cells. At the same concentration, the cytotoxicities of the precursors follow the order of **1p** > **5p** > **7p** at all concentrations, agreeing with the amount of assemblies formed via EISA (vide supra). When the concentration of **5p** increases from 20 to 50 μM, there is a significant decrease of cell viability. This observation correlates well with the fact that there are significantly more assemblies at 50 μM **5p** after dephosphorylation (Figure S22, SI). The increase of concen-

DOI: 10.1021/jacs.7b07147
J. Am. Chem. Soc. 2017, 139, 15377−15384

tration results in the enhanced cytotoxicity of **1p** and **5p**, positively correlating with the increase of the assemblies. These results indicate that the self-assembling abilities of these molecules determine the efficacy of EISA for inhibiting Saos-2 cells because higher self-assembling ability results in more assemblies at a constant concentration of the precursors. Remarkably, 8.8 μg/mL of **1p** inhibits over 90% of Saos-2 cells (Figure S23, SI). This IC_{90} value of **1p** against Saos-2 cells is comparable to or, in fact, even more potent than the clinically used drug (cisplatin) for treating osteosarcoma.[42]

Inhibitory Activities against Different Cell Lines. In addition to Saos-2 cells, we also examined the cytotoxicity of **1p** and **5p** on different cancer cell lines [breast adenocarcinoma cells (MCF-7) and glioblastoma cells (T98G)] and a normal stromal cell line (HS-5). (Figure 5) In contrast to the case of Saos-2 cells,

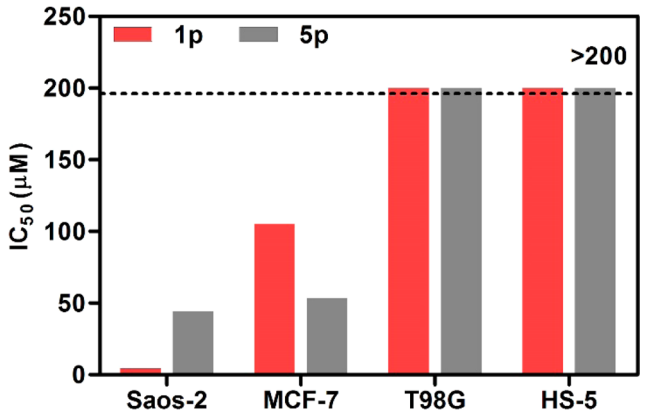

Figure 5. IC_{50} (72 h) of **1p** or **5p** against Saos-2 cells, MCF-7 cells, T98G cells, or HS-5 cells.

5p shows a higher inhibition effect than **1p** on MCF-7 cells. The IC_{50} of **5p** on MCF-7 is 47.0 μg/mL (53.5 μM), while the IC_{50} of **1p** is 92.4 μg/mL (105 μM). This result likely results from the hydrolysis of the methyl ester bond of **1p**, since MCF-7 cells express relatively high level of carboxylesterases.[9] In addition, the IC_{50} of **1p** (>176 μg/mL) (200 μM)[28] on HepG2 cells, which are known to greatly overexpress esterase, is 2-fold the IC_{50} of **5p** (92.4 μg/mL) (111 μM) (Figure S24, SI). The hydrolysis of the ester on **1** would generate **1″** (vide infra), which possesses much lower self-assembling ability. While the precursors potently inhibit Saos-2 cells with an IC_{50} value of 3.9 μg/mL (4.4 μM) for **1p** and 38.9 μg/mL (44.3 μM) for **5p**, they scarcely exhibit cytotoxicities to T98G or HS-5 cells, even at the concentration of 176 μg/mL (200 μM). This result agrees with the low expression level of ALP on these two cell lines,[10] further confirming that the selective inhibition of EISA precursors against cancer cells originates from the expression level of enzymes and the rate of self-assembly resulted from the enzymatic reaction.

Molecular Transformation in Cellular Milieu. To reveal the molecular transformation and self-assembly of EISA molecules in cellular milieu, we coincubated **1p** or **5p** with Saos-2 cells, HepG2 cells, or HS-5 cells and quantified the conversion of the precursors after 24 h incubation (Figure 6). LC−MS and HPLC analyses show that the endogenous ALP turns **1p** into **1**, carboxylesterase (CES) converts **1p** to **1p′**, and catalysis by ALP and CES yields **1″**, while the **5p** only transforms into **5** by ALP, due to the stability of methyl amide (Figures S25−S27, SI). As shown in Figure 6A, 15.2%, 46.9%, and 62.2% of **1p** molecules remain in Saos-2, HepG2, and HS-5 cells, respectively,

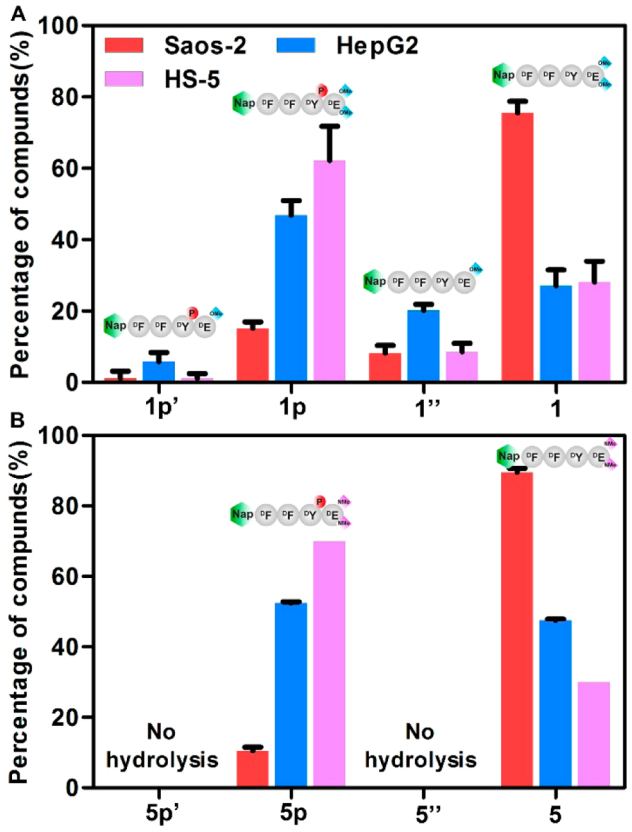

Figure 6. (A) Percentage of compounds **1p′** (hydrolysis product of **1p**), **1p**, **1″**, and **1** after incubating **1p** (200 μM) with Saos-2 cells, HepG2 cells, or HS-5 cells. (B) Percentage of compounds **5p′** (hydrolysis product of **5p**), **5p**, **5″**, and **5** after incubating **5p** (200 μM) with Saos-2 cells, HepG2 cells, or HS-5 cells. The ratios were determined using HPLC and LC−MS. Cells were treated for 24 h.

indicating that the activities of ALP on these cells follow the order of Saos-2 > HepG2 > HS-5,[10] which is also consistent with the cytotoxicity of **1p** for these cell lines. Although HepG2 exhibits higher ALP activity than HS-5, its high expression level of CES results in hydrolyzing 26% of carboxyl methyl ester, which is over twice of the same hydrolysis on HS-5 cells (i.e., 9.7%). As a result, the amount of self-assembling molecule **1** in the cultures for Saos-2, HepG2, and HS-5 are 75.5%, 27.1%, and 28.1%, respectively. Because of the much poorer self-assembling ability of **1″** compared with that of **1**, these results explain that **1p** potently inhibits Saos-2 cells, but it is innocuous to HepG2 cells.

In addition, ALPs on Saos-2, HepG2, and HS-5 cells convert 89.6%, 47.6%, and 30.0% of **5p** to **5**, respectively, further confirming that the activities of ALP follow the order of Saos-2 > HepG2 > HS-5. For **1p** and **5p**, Saos-2 cells dephosphorylate comparable amounts of the precursors (i.e., 66.2% for **1** and 75.5% for **5**), supporting that the inhibitory efficacy follows the trend of self-assembling ability. For HepG2 cells, the total amount (i.e., 47.3%) of **1** and **1″** is almost same as the generation of **5** (i.e., 47.6%). However, the **1**/**1″** molar ratios in the cultures of HepG2 cells are 27.1/20.2. Together with the cytotoxicity data, these results suggest that the amount of the assemblies (made of **1** and **1″**, or **5**), in fact, determines the efficacy of EISA. These detailed results of the conversion of the EISA molecules, indeed, reveal the complexity of EISA in cell milieu, which underscores the importance of correlating the self-assembling

DOI: 10.1021/jacs.7b07147
J. Am. Chem. Soc. 2017, 139, 15377−15384

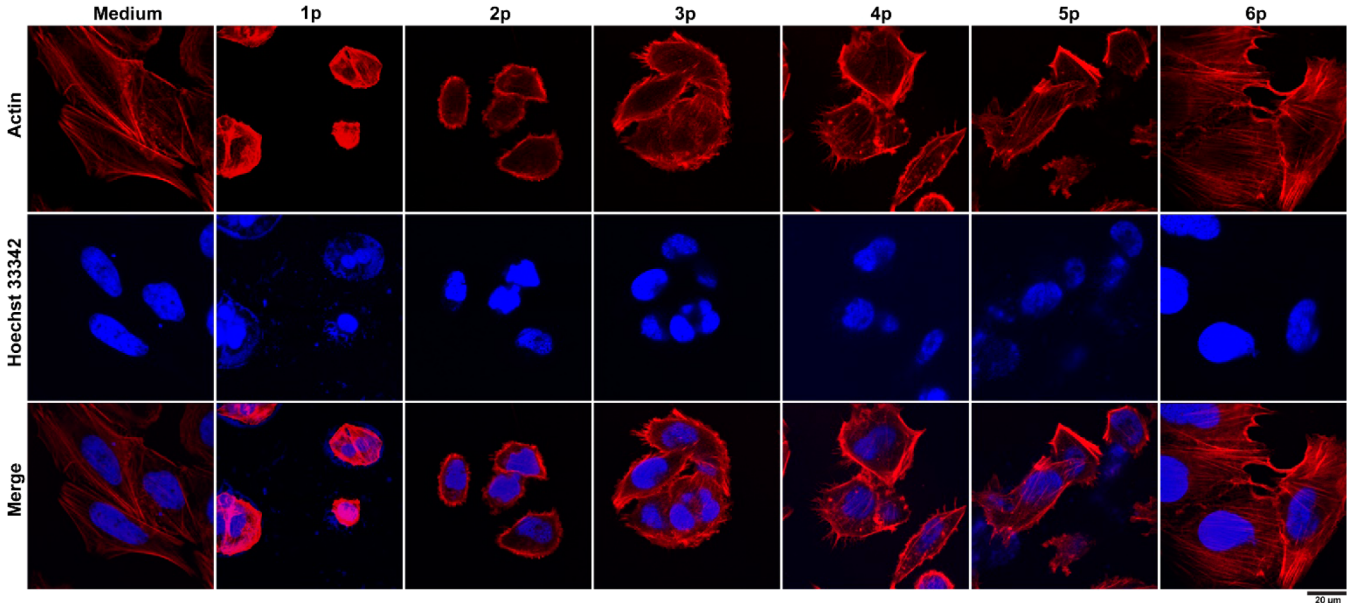

Figure 7. CLSM images of Saos-2 cells stained with Alexa Fluor 633 Phalloidin (F-actin, red) and Hoechst (nuclei, blue) after the treatment of culture medium, **1p**, **2p**, **3p**, **4p**, **5p**, or **6p** for 12 h. Scale bars = 20 μm.

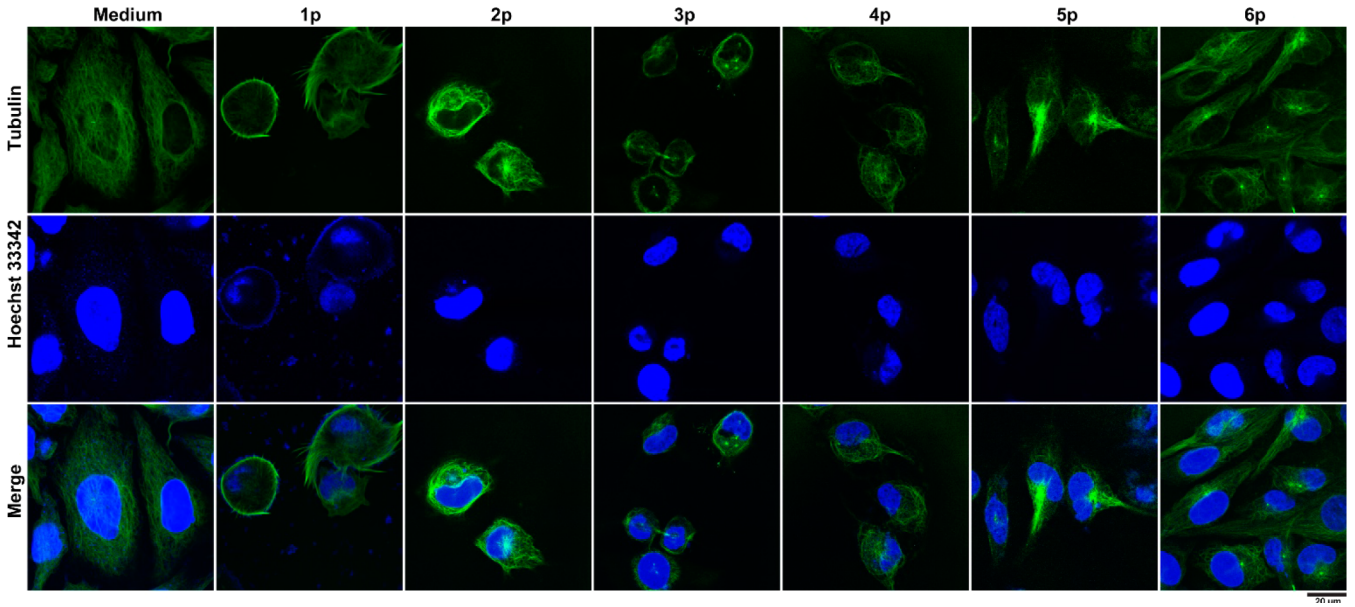

Figure 8. CLSM images of Saos-2 cells stained with tubulin tracker (green) and Hoechst (nuclei, blue) after the treatment of culture medium, **1p**, **2p**, **3p**, **4p**, **5p**, and **6p** for 12 h. Scale bars = 20 μm.

ability of *stable* molecules with the efficacy of EISA for inhibiting cancer cells.

Mechanism of Cell Death. To confirm that the EISA processes play critical roles in the inhibitory effect, we coincubated the precursor **1p** and exogenous ALP or a tissue-nonspecific alkaline phosphatase (TNAP) inhibitor[43] with Saos-2 cells. Both exogenous ALP and the TNAP inhibitor rescue the cells, increasing the cell viability from 11% to 69% and 23%, respectively (Figure S28, SI). This result validates the contribution of EISA processes. The TNAP inhibitor 2,5-dimethoxy-*N*-(quinolin-3-yl)benzenesulfonamide (DQB) only inhibits TNAP effectively,[43] so it is unlikely that it would completely rescue the cells due to the presence of other isozymes of ALP[44] on the cells or other phosphatases in cell milieu. The addition of pan-caspase inhibitor (zVAD-fmk)[45] or necroptosis inhibitor (Nec-1)[46] increases the cell viability of Saos-2 cells treated with the **1p** to 25% or 32%, respectively (Figure S28, SI), indicating that either apoptosis or necroptosis represents a path to the death of Saos-2 treated by **1p**, though other death pathways remain to be validated. In addition, Congo red staining results reveal that the precursors (**1p** and **5p**) form assemblies both pericellularly and intracellularly via EISA (Figure S29, SI). Congo red is unable to stain the apoptotic Saos-2 cells induced by cisplatin (Figure S30, SI), further confirming that the staining of Saos-2 cells incubated with EISA molecules by Congo red originates from the assemblies of the EISA molecules (e.g., **1** or **5**).

The EISA of **1p**/**1** also leads to the morphology change of Saos-2 cells, indicating that the resulting assemblies affect the integrity of the cytoskeletons. We stained the F-actin with Alexa

DOI: 10.1021/jacs.7b07147
J. Am. Chem. Soc. 2017, 139, 15377−15384

Fluor 633 Phalloidin to reveal the shape changes. The staining results (Figure 7) show that the treatments of precursors disrupt the F-actin arrangement, while the control Saos-2 cells exhibit stretched thin actin filaments. The treatment of **1p** and **2p** results in significant shrinkage of actin networks and much higher density of F-actin at the cell boundary. Notably, the actin filaments are much shorter in the cells treated with **2p**. Similarly, **3p**−**5p** also cause the accumulation of actin near plasma membranes, reflecting the increase of focal adhesion and the decrease of fibrillar adhesion of cells.[47] Different from the control cells, the actin filaments become much shorter or punctate upon the treatment with **3p**, **4p**, or **5p**. However, **6p** shows little effect on the actin of Saos-2 cells, likely due to the poor self-assembling ability of **6**. The gradual change of the actin morphology upon the treatment of the precursors from **1p** to **6p** indicates that the assemblies of the peptide derivatives likely disrupt actin dynamics and cause the cell death.

To get more insights on how the EISA process affects the cytoskeletons, we also evaluated the changes of microtubules upon the treatment of the precursors. As shown in Figure 8, **1p** leads to the reorganization of microtubules in the proximity of plasma membranes of Saos-2 cells, which likely corresponds with the apoptotic microtubule network (AMN)[48] formed during the execution phase of apoptosis. This result supports that the treatment of **1p** is able to cause apoptosis. The microtubules of Saos-2 cells become shorter and accumulate near the cell boundary after incubation with **2p** or **3p**. In addition, **2p**, **3p**, **4p**, or **5p** causes tubulins to aggregate at the centromere in Saos-2 cells, while **6p** hardly influences the morphology of microtubules. Moreover, the live cell imaging shows that the addition of **1p** rapidly leads to the membrane blebbing of Saos-2 cells and reorganization of plasma membrane followed by the loss of focal adhesion,[49] agreeing with the disruption of cytoskeleton dynamics resulting in cell death.

The addition of TNAP inhibitor (DQB) reduces the formation of nanofibers of **1** on Saos-2 cells (Figure S31, SI) and lessens the disruption of cytoskeletons (Figures S33 and 34, SI), further supporting the critical role of TNAP for EISA in inducing Saos-2 cell death. In addition, increasing the concentration of DQB reduces nanofiber formation (Figure S31, SI), suggesting that the inhibition of dephosphorylation depends on the concentration of DQB, which is supported by the higher concentrations of DQB rescuing more Saos-2 cells coincubated with **1p** (Figure S32, SI). Incubating HS-5 cells with the self-assembling molecule **1**, we examine the effect of hydrogelator on the normal cells. The Congo red staining results reveal that the assemblies of **1** hardly accumulate on HS-5 cells, even at the concentration of 100 μM. (Figure S35, SI) Moreover, **1** exhibits little effect on the cytoskeletons of HS-5 cells, at concentrations both below (i.e., 2 μM) and above (i.e., 10 μM) its cmc (2.7 μM) (Figures S36 and 37, SI). Only when the concentration is high enough (i.e., 100 μM), **1** starts to show slight disruptions on the cytoskeletons of HS-5 cells (Figures S36 and 37, SI).

CONCLUSION

In conclusion, this study establishes the self-assembling ability of EISA molecules as a key thermodynamic parameter for determining the efficacy of EISA against cancer cells that overexpresses certain enzymes. As revealed by the time-dependent dephosphorylation experiment (Figure S38, SI), the dephosphorylation rate of precursor **1p** largely depends on the concentration of enzymes. This result indicates that, while the self-assembling ability determines the thermodynamic properties of EISA, the enzyme expression (and genetic information[50]) of cancer cells kinetically controls the EISA process. Taken together, these two parameters suggest that it is feasible to obtain the thermodynamic and kinetic properties of the EISA molecules in cell-free assays to predict the efficacy of EISA. Moreover, the understanding of the molecular transformation of the precursors in cell milieu (e.g., Figure 6) not only highlights the complexity of cells but also illustrates how multiple enzymes control the EISA process to enable precise regulation of the formation of the assemblies in different cellular environments. In fact, the rapid dephosphorylation results in quick building up of the assemblies, which likely hampers the hydrolysis of the diesters (Figure S39, SI). Such kinetic control may be particularly useful for selectively targeting the desired cancer cells,[51] thus greatly reducing the off-target effects of assemblies. Although in this work we demonstrate the use of EISA for inhibiting cancer cells, the insights obtained here should be applicable to other applications, like molecular imaging,[25,52] analyte detection,[53] and vaccine adjuvants,[6] as well as the understanding of cytotoxicity of pathogenic assemblies (e.g., β-amyloids).[54] Moreover, the recent advances in structural biology and cell biology have revealed that nature uses a dynamic continuum of protein assemblies to control cellular processes.[55] Thus, this work also underscores a thermodynamic aspect for developing a dynamic continuum of supramolecular nanostructures as a functional mimic of higher-order protein assemblies.

ASSOCIATED CONTENT

Supporting Information

The Supporting Information is available free of charge on the ACS Publications website at DOI: 10.1021/jacs.7b07147.

Materials and detailed experimental procedures and additional figures (Figures S1−S39 and Table S1) (PDF)

AUTHOR INFORMATION

Corresponding Author

*bxu@brandeis.edu

ORCID

Huaimin Wang: 0000-0002-8796-0367

Bing Xu: 0000-0002-4639-387X

Notes

The authors declare no competing financial interest.

ACKNOWLEDGMENTS

This work was partially supported by NIH (R01CA142746) and NSF (DMR-1420382).

REFERENCES

(1) Hopkins, A. L.; Groom, C. R. *Nat. Rev. Drug Discovery* **2002**, *1*, 727.

(2) Verdine, G. L.; Walensky, L. D. *Clin. Cancer Res.* **2007**, *13*, 7264.

(3) Makley, L. N.; Gestwicki, J. E. *Chem. Biol. Drug Des.* **2013**, *81*, 22.

(4) Carlier, M. F. *Philos. Trans. R. Soc., B* **1992**, *336*, 93.

(5) Li, J.; Kuang, Y.; Gao, Y.; Du, X.; Shi, J.; Xu, B. *J. Am. Chem. Soc.* **2013**, *135*, 542. Yang, Z.; Liang, G.; Guo, Z.; Guo, Z.; Xu, B. *Angew. Chem., Int. Ed.* **2007**, *46*, 8216.

(6) Wang, H.; Luo, Z.; Wang, Y.; He, T.; Yang, C.; Ren, C.; Ma, L.; Gong, C.; Li, X.; Yang, Z. *Adv. Funct. Mater.* **2016**, *26*, 1822.

(7) Kuang, Y.; Shi, J. F.; Li, J.; Yuan, D.; Alberti, K. A.; Xu, Q. B.; Xu, B. *Angew. Chem., Int. Ed.* **2014**, *53*, 8104.

DOI: 10.1021/jacs.7b07147
J. Am. Chem. Soc. 2017, 139, 15377−15384

(8) Li, J.; Kuang, Y.; Shi, J.; Zhou, J.; Medina, J. E.; Zhou, R.; Yuan, D.; Yang, C.; Wang, H.; Yang, Z.; Liu, J.; Dinulescu, D. M.; Xu, B. *Angew. Chem., Int. Ed.* **2015**, *54*, 13307. Kalafatovic, D.; Nobis, M.; Son, J.; Anderson, K. I.; Ulijn, R. V. *Biomaterials* **2016**, *98*, 192.
(9) Li, J.; Shi, J.; Medina, J. E.; Zhou, J.; Du, X.; Wang, H.; Yang, C.; Liu, J.; Yang, Z.; Dinulescu, D. M.; Xu, B. *Adv. Healthcare Mater.* **2017**, *6*, 1601400.
(10) Zhou, J.; Du, X. W.; Yamagata, N.; Xu, B. *J. Am. Chem. Soc.* **2016**, *138*, 3813.
(11) Feng, Z. Q. Q.; Wang, H. M.; Du, X. W.; Shi, J. F.; Li, J.; Xu, B. *Chem. Commun.* **2016**, *52*, 6332.
(12) Du, X.; Zhou, J.; Wang, H.; Shi, J.; Kuang, Y.; Zeng, W.; Yang, Z.; Xu, B. *Cell Death Dis.* **2017**, *8*, e2614. Wang, H.; Feng, Z.; Wu, D.; Fritzsching, K. J.; Rigney, M.; Zhou, J.; Jiang, Y.; Schmidt-Rohr, K.; Xu, B. *J. Am. Chem. Soc.* **2016**, *138*, 10758.
(13) Fishman, W. H.; Inglis, N. R.; Green, S.; Anstiss, C. L.; Gosh, N. K.; Reif, A. E.; Rustigian, R.; Krant, M. J.; Stolbach, L. L. *Nature* **1968**, *219*, 697.
(14) Zhang, Z. Y. *Acc. Chem. Res.* **2017**, *50*, 122.
(15) Zhou, J.; Xu, B. *Bioconjugate Chem.* **2015**, *26*, 987.
(16) Wang, H.; Feng, Z.; Wang, Y.; Zhou, R.; Yang, Z.; Xu, B. *J. Am. Chem. Soc.* **2016**, *138*, 16046.
(17) Bourzac, K. *Nature* **2014**, *509*, S69.
(18) Pires, R. A.; Abul-Haija, Y. M.; Costa, D. S.; Novoa-Carballal, R.; Reis, R. L.; Ulijn, R. V.; Pashkuleva, I. *J. Am. Chem. Soc.* **2015**, *137*, 576.
(19) Tanaka, A.; Fukuoka, Y.; Morimoto, Y.; Honjo, T.; Koda, D.; Goto, M.; Maruyama, T. *J. Am. Chem. Soc.* **2015**, *137*, 770.
(20) Zheng, Z.; Chen, P. Y.; Xie, M. L.; Wu, C. F.; Luo, Y. F.; Wang, W. T.; Jiang, J.; Liang, G. L. *J. Am. Chem. Soc.* **2016**, *138*, 11128.
(21) Wang, H. M.; Luo, Z.; Wang, Y. C. Z.; He, T.; Yang, C. B.; Ren, C. H.; Ma, L. S.; Gong, C. Y.; Li, X. Y.; Yang, Z. M. *Adv. Funct. Mater.* **2016**, *26*, 1822.
(22) Conley, N. R.; Dragulescu-Andrasi, A.; Rao, J. H.; Moerner, W. E. *Angew. Chem., Int. Ed.* **2012**, *51*, 3350.
(23) Lin, Y. X.; Qiao, S. L.; Wang, Y.; Zhang, R. X.; An, H. W.; Ma, Y.; Rajapaksha, R.; Qiao, Z. Y.; Wang, L.; Wang, H. *ACS Nano* **2017**, *11*, 1826.
(24) Du, X. W.; Zhou, J.; Wang, J. Q.; Zhou, R.; Xu, B. *ChemNanoMat* **2017**, *3*, 17.
(25) Dong, L.; Qian, J.; Hai, Z.; Xu, J.; Du, W.; Zhong, K.; Liang, G. *Anal. Chem.* **2017**, *89*, 6922.
(26) Lock, L. L.; Reyes, C. D.; Zhang, P. C.; Cui, H. G. *J. Am. Chem. Soc.* **2016**, *138*, 3533. Wen, Y.; Waltman, A.; Han, H. F.; Collier, J. H. *ACS Nano* **2016**, *10*, 9274. Li, S.; Mehta, A. K.; Sidorov, A. N.; Orlando, T. M.; Jiang, Z. G.; Anthony, N. R.; Lynn, D. G. *J. Am. Chem. Soc.* **2016**, *138*, 3579. Magnotti, E. L.; Hughes, S. A.; Dillard, R. S.; Wang, S. Y.; Hough, L.; Karumbamkandathil, A.; Lian, T. Q.; Wall, J. S.; Zuo, X. B.; Wright, E. R.; Conticello, V. P. *J. Am. Chem. Soc.* **2016**, *138*, 16274. Sato, K.; Ji, W.; Palmer, L. C.; Weber, B.; Barz, M.; Stupp, S. I. *J. Am. Chem. Soc.* **2017**, *139*, 8995. Hamley, I. W. *Chem. Rev.* **2012**, *112*, 5147. Burgess, N. C.; Sharp, T. H.; Thomas, F.; Wood, C. W.; Thomson, A. R.; Zaccai, N. R.; Brady, R. L.; Serpell, L. C.; Woolfson, D. N. *J. Am. Chem. Soc.* **2015**, *137*, 10554. Zhang, S. G. *Acc. Chem. Res.* **2012**, *45*, 2142. Yoo, S. P.; Pineda, F.; Barrett, J. C.; Poon, C.; Tirrell, M.; Chung, E. J. *ACS Omega* **2016**, *1*, 996. Li, I. C.; Hartgerink, J. D. *J. Am. Chem. Soc.* **2017**, *139*, 8044. Ardoña, H. A. M.; Draper, E. R.; Citossi, F.; Wallace, M.; Serpell, L. C.; Adams, D. J.; Tovar, J. D. *J. Am. Chem. Soc.* **2017**, *139*, 8685. Nagy, K. J.; Giano, M. C.; Jin, A.; Pochan, D. J.; Schneider, J. P. *J. Am. Chem. Soc.* **2011**, *133*, 14975.
(27) Wang, H. M.; Feng, Z. Q. Q.; Xu, B. *Chem. Soc. Rev.* **2017**, *46*, 2421.
(28) Feng, Z.; Wang, H.; Zhou, R.; Li, J.; Xu, B. *J. Am. Chem. Soc.* **2017**, *139*, 3950.
(29) Reches, M.; Gazit, E. *Nat. Nanotechnol.* **2006**, *1*, 195.
(30) Yang, Z. M.; Gu, H. W.; Fu, D. G.; Gao, P.; Lam, J. K.; Xu, B. *Adv. Mater.* **2004**, *16*, 1440.
(31) Hancock, J. F.; Cadwallader, K.; Marshall, C. J. *EMBO J.* **1991**, *10*, 641−646.
(32) Van Damme, P.; Arnesen, T.; Gevaert, K. *FEBS J.* **2011**, *278*, 3822.
(33) Alewood, P. F.; Johns, R. B.; Valerio, R. M.; Kemp, B. E. *Synthesis* **1983**, *1983*, 30.
(34) Ottinger, E. A.; Shekels, L. L.; Bernlohr, D. A.; Barany, G. *Biochemistry* **1993**, *32*, 4354.
(35) Merrifield, R. B. *J. Am. Chem. Soc.* **1963**, *85*, 2149.
(36) Brook, M. A.; Chan, T. H. *Synthesis* **1983**, *1983*, 201.
(37) Carey, M. C.; Small, D. M. *J. Colloid Interface Sci.* **1969**, *31*, 382.
(38) Marrink, S. J.; Tieleman, D. P.; Mark, A. E. *J. Phys. Chem. B* **2000**, *104*, 12165. Sadownik, J. W.; Leckie, J.; Ulijn, R. V. *Chem. Commun.* **2011**, *47*, 728.
(39) Murray, E.; Provvedini, D.; Curran, D.; Catherwood, B.; Sussman, H.; Manolagas, S. *J. Bone Miner. Res.* **1987**, *2*, 231.
(40) Marsh, D. *Biophys. J.* **2012**, *102*, 1079.
(41) Stewart, M. J.; Watson, I. D. *Br. J. Clin. Pharmacol.* **1983**, *16*, 3.
(42) Voss, C.; Eyol, E.; Berger, M. R. *Toxicol. Appl. Pharmacol.* **2006**, *211*, 177.
(43) Dahl, R.; Sergienko, E. A.; Su, Y.; Mostofi, Y. S.; Yang, L.; Simao, A. M.; Narisawa, S.; Brown, B.; Mangravita-Novo, A.; Vicchiarelli, M.; Smith, L. H.; O'Neill, W. C.; Millan, J. L.; Cosford, N. D. P. *J. Med. Chem.* **2009**, *52*, 6919.
(44) Fishman, W. H. *Clin. Biochem.* **1990**, *23*, 99.
(45) Slee, E. A.; Zhu, H. J.; Chow, S. C.; MacFarlane, M.; Nicholson, D. W.; Cohen, G. M. *Biochem. J.* **1996**, *315*, 21.
(46) Degterev, A.; Huang, Z. H.; Boyce, M.; Li, Y. Q.; Jagtap, P.; Mizushima, N.; Cuny, G. D.; Mitchison, T. J.; Moskowitz, M. A.; Yuan, J. Y. *Nat. Chem. Biol.* **2005**, *1*, 112.
(47) Geiger, B.; Yamada, K. M. *Cold Spring Harbor Perspect. Biol.* **2011**, *3*, a005033.
(48) Sanchez-Alcazar, J. A.; Rodriguez-Hernandez, A.; Cordero, M. D.; Fernandez-Ayala, D. J. M.; Brea-Calvo, G.; Garcia, K.; Navas, P. *Apoptosis* **2007**, *12*, 1195.
(49) Xu, B. Unpublished work, 2017.
(50) Zhou, J.; Du, X. W.; Berciu, C.; He, H. J.; Shi, J. F.; Nicastro, D.; Xu, B. *Chem* **2016**, *1*, 246.
(51) Zhou, J.; Du, X. W.; Xu, B. *Angew. Chem., Int. Ed.* **2016**, *55*, 5770.
(52) Nejadnik, H.; Ye, D. J.; Lenkov, O. D.; Donig, J. S.; Martin, J. E.; Castillo, R.; Derugin, N.; Sennino, B.; Rao, J. H.; Daldrup-Link, H. *ACS Nano* **2015**, *9*, 1150.
(53) Yuan, Y.; Ge, S. C.; Sun, H. B.; Dong, X. J.; Zhao, H. X.; An, L. N.; Zhang, J.; Wang, J. F.; Hu, B.; Liang, G. L. *ACS Nano* **2015**, *9*, 5117. Shigemitsu, H.; Fujisaku, T.; Onogi, S.; Yoshii, T.; Ikeda, M.; Hamachi, I. *Nat. Protoc.* **2016**, *11*, 1744.
(54) Song, Y.; Moore, E. G.; Guo, Y.; Moore, J. S. *J. Am. Chem. Soc.* **2017**, *139*, 4298. Limbocker, R.; Mannini, B.; Perni, M.; Chia, S.; Heller, G.; Ruggeri, F. S.; Habchi, J.; Meisl, G.; Challa, P. K.; Zasloff, M.; Knowles, T. P. J.; Vendruscolo, M.; Dobson, C. M. *Biophys. J.* **2017**, *112*, 494a. Colvin, M. T.; Silvers, R.; Ni, Q. Z.; Can, T. V.; Sergeyev, I.; Rosay, M.; Donovan, K. J.; Michael, B.; Wall, J.; Linse, S.; Griffin, R. G. *J. Am. Chem. Soc.* **2016**, *138*, 9663. Zhou, R.; Xu, B. *PLoS One* **2014**, *9*, e95759.
(55) Wu, H.; Fuxreiter, M. *Cell* **2016**, *165*, 1055.

DOI: 10.1021/jacs.7b07147
J. Am. Chem. Soc. 2017, 139, 15377−15384